Geothermal Energy

RESEARCH Open Access

Experimental assessment of sealing integrity of grouts and clay pellets under thermal cycles representative of HT-ATES operation

Alexis Koulidis[1*], Martin Bloemendal[1,2] and Philip J. Vardon[1]

*Correspondence:
k.a.koulidis@tudelft.nl

[1] Faculty of Civil Engineering and Geosciences, Delft University and Technology, Delft, The Netherlands
[2] TNO, Dutch Geological Survey, Utrecht, The Netherlands

Abstract

High-temperature aquifer thermal energy storage (HT-ATES) can play a key role in the energy transition. For well completion of conventional low-temperature ATES and groundwater wells, grout and/or clay pellets are typically utilised as annular materials to ensure the long-term well integrity. It is not yet known if such materials can also be used in HT-ATES working conditions. In this work, a novel approach to evaluate the sealing performance for such completion materials is proposed and tested over multiple thermal heating and cooling cycles representative of the conditions of HT-ATES operation. The experimental framework utilises a novel experimental design to test the apparent transmissivity of the annular material, followed by micro-CT scanning. During each test, up to 11 thermal cycles are applied, with temperature variations between 22^{o}C and 90^{o}C. For grouts after 7 days of curing, micro-CT scans reveal debonding and the occurrence of micro-annuli with an equivalent diameter of approximately 26% of the original cross-section. After 28 days of curing, the thermal cycles had a much reduced impact on micro-annulus formation. The corresponding apparent transmissivity decreased up to 80% for samples containing a high percentage of cementitious minerals and a low water-to-grout ratio. The clay pellets, saturated with fresh water, demonstrated effective sealing capacity and an impermeable behaviour. However, clay pellets saturated with 0.25 mol/L NaCl, showed up to an 85% decrease in swelling capacity yet still exhibited impermeable behaviour. The results indicated that thermal cycles affect the integrity of grouts, while clay pellets show resilience to them. Furthermore, longer curing periods and specific chemical compositions improve sealing performance and provide resilience to thermal cycles.

Keywords: High temperature, Aquifer thermal energy storage, Heat storage wells, Sealing performance, Grouts, Micro-annulus, Clay pellets, Transmissivity

Introduction

The high thermal energy demand and the desired reduction in the use of fossil fuels have accelerated the development of the use of sustainable sources of thermal energy such as geothermal energy, solar energy, waste heat and/or power-to-heat. Such sustainable sources of thermal energy typically have a temporal mismatch with demand for heating. Geothermal energy, for example, can be produced year-round, whereas the thermal

energy demand is high in the winter and low in the summer. For solar, the mismatch is even larger, where most energy is produced in summer and little in winter. Therefore, underground thermal energy storage, which has large capacities suitable for seasonal storage, has a key role in the energy transition (Oesterholt et al 2018; Bloemendal et al 2021). High-temperature aquifer thermal energy storage (HT-ATES) systems are a promising technology for large-scale and seasonal thermal energy storage, and have a higher energy density than conventional ATES systems. They involve storing and retrieving large volumes of hot water (Birdsell et al 2021; Daniilidis et al 2022), as shown in Figure 1.

To have low capital and operation costs, HT-ATES systems proposed are mostly at depths limited to a few hundreds of metres in sedimentary systems, i.e. permeable, sandy layers with groundwater (aquifers) accessible through tube wells (Bloemendal and Hartog 2018; Dinkelman and Bergen 2022). The early adopters of this technology have based well designs on conventional ATES or groundwater wells (Bloemendal et al 2020; Dinkelman et al 2022), considering pump, screen and casing materials that can withstand higher temperatures (Zwamborn et al 2022). However, during the completion of a conventional ATES or groundwater well (cylindrical boreholes), the annular space between the borehole and the casing is also backfilled. Usually, gravel is used at the well screen interval and an impermeable material around the closed casing (van't Westende and Willems 2022). The goal of the impermeable annular completion material for any groundwater well is to seal the annulus between the casing and the drilled hole to prevent short-circuit flow of groundwater between aquifers through impermeable layers penetrated by the well drilling (Ogden and Ruff 1991). In the Netherlands, the required hydraulic conductivity of the backfilling materials is required to be less than 10^{-9} m/s (van der Schans 2021; SIKB 2021).

In conventional low-temperature ATES systems, the sealing materials are normally subjected to small variations in temperature (Pellegrini et al 2019), which corresponds to low variations in stress and strain due to thermal expansion. HT-ATES systems are designed to have temperatures up to around 90^{o}C, which the well is exposed to during

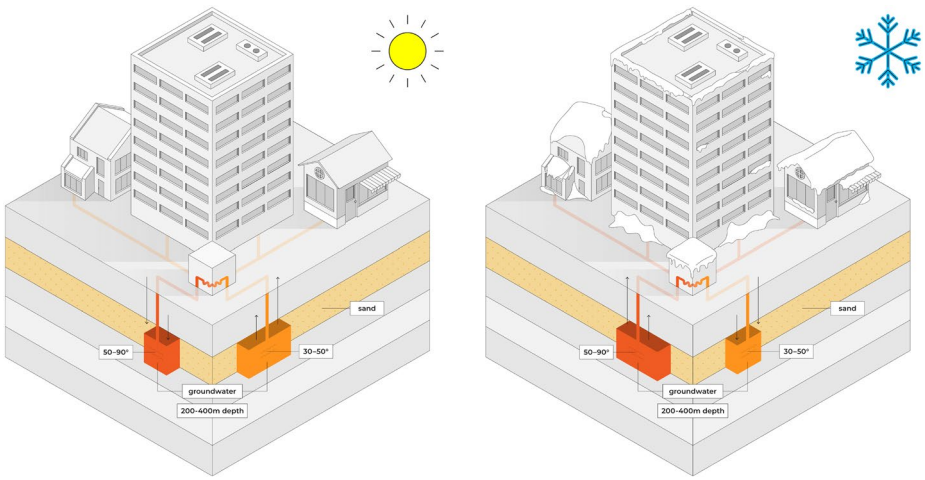

Fig. 1 HT-ATES operation system. Left: heat injection during summer time into the hot well; right: heat extraction from the hot well during winter time and injection into the cold well (PUSH-IT 2025)

injection and extraction. However, the temperatures can be substantially lower during periods that the system is idle, and will cool down to the much low surrounding in situ temperatures. Therefore, both higher thermally induced stress and strain, and cyclic behaviour are expected. Hence, to ensure the integrity of HT-ATES wells, selecting an annular material which is capable of maintaining high sealing capacity while experiencing large temperature variations is essential.

Among the different types of annular materials, grout is commonly used for shallow depth applications (Mahmoud et al 2021). Grouts are defined by their relatively low viscosity, which ensures good pumpability (Zhang et al 2019), making them preferred for shallow applications. The composition of grouts primarily consists of cement, bentonite and additional components, which can include sand and graphite, which yields thermal conductivities ranging from 0.75 W/mK up to 3 W/mK (Lee et al 2010, 2011). The mechanical properties are influenced by the composition of the mixture and the water-to-grout ratio (Marshland 1973), with cement replacement materials, e.g. fly ash (calcium and gypsum), being known to reduce the strength and stiffness (Mikkelsen 2002).

In groundwater and ATES wells, granular clay pellets are a common annular material utilised as a barrier because of their practicality (Darde et al 2021). The thermal conductivity of dry clay pellets is significantly lower compared to grout, with values measured to be below 0.2 W/mK (Laterlite 2025). The clay pellets are pumped with the assistance of gravity into the annulus through a tube in dry conditions (Ogden and Ruff 1991, 1993). Upon contact with groundwater, the hydration process is initiated, causing the pellets to swell and lose their granular geometry (Guerra et al 2018), which results in filling the annulus and a low bulk hydraulic conductivity. The particle size distribution of the clay pellets has a major effect on the packing density and corresponding swelling capacity (Liu et al 2019; Qin et al 2024), and therefore the sealing capacity.

The rapid swelling capacity makes clay pellet implementation challenging for deeper wells, potentially leading to misplacement in the wellbore (Ogden and Ruff 1991). Coating of the clay pellets prior to the placement in the borehole has been shown to retard the swelling, allowing the pellets to reach the target depth before swelling starts (Top Sector Energie 2018). Therefore, there has been limited research on applications in higher temperature situations. Various cement mortars are used in the annular space of deep boreholes for geothermal and oil/gas wells to ensure long-term well integrity. Cement slurry is cured under different conditions along the borehole, and many studies have been performed to evaluate the integrity of the cement sheath (Goodwin and Crook 1992; Shadravan et al 2015; Li et al 2016; Kiran et al 2017). However, cement mortars are substantially more expensive than grouts or clay pellets and have related carbon emissions in production and therefore, if possible, are avoided in shallow boreholes.

HT-ATES wells are subjected to (high amplitude) cyclic heating and cooling. During production or injection, the casing is heated by the production or injection fluid, and the casing expands (Lavrov et al 2016). The rate at which the metal expands is a function of the thermal expansion coefficient. The casing expansion applies thermal stress to the annular material (Thiercelin et al 1998; Lavrov et al 2016; Xu et al 2018; Wu et al 2020). Thermal loading has been observed to create mechanical stress in annular cement, causing debonding and the formation of a micro-annulus, as a result compromising the well integrity (Teodoriu and Falcone 2009; Bois et al 2011, 2012; Shadravan et al 2015; Roy

et al 2018). Ichim and Teodoriu (2017) developed an experimental framework to assess cement behaviour under thermal cycles, with the results indicating that for short curing periods (i.e. less than 21 days), temperature cycles enhanced the uniaxial compressive strength. Fischer and Moghadam (2023) performed thermal cycles between 100^{o}C and 18^{o}C on a cement, with the samples not showing any obvious damage. Similarly, De Andrade et al (2015) showed that tensile cracks were the main cause of failure upon thermal cycles, noting no significant debonding. There are no similar works examining the performance of grouts or clay pellets commonly used in shallower wells, a gap which this work aims to address.

Specifically, the performance of grouts and clay pellets exposed to temperature cycles is studied in this paper. This work replicates relevant temperature-cycle scenarios in a laboratory setup for application in HT-ATES systems, i.e. high amplitude temperature cycles. The objective is to experimentally evaluate the effect of heating and cooling cycles on the sealing capacity of grout and clay pellet materials for high-temperature and low-stress conditions. To this end, a novel method is developed and tested to measure the apparent transmissivity of annular material, reflecting the sealing capacities. Measurements before and after thermal cycles, in combination with micro-CT scans, allows the determination of the extent to which the completion materials are suitable for HT-ATES.

Materials used for backfilling and their characteristics

Grouts

The experiments utilise commercially available grout materials commonly used for the completion of various shallow drilling operations. Three products are tested in this study with permission for testing from the manufacturers. The suppliers provided partial thermal and mechanical properties and chemical composition. To ensure comparability, these are again measured. The grout mixtures consist of mixed components: cementation minerals, clay minerals, graphite and quartz. X-ray diffraction (XRD) analysis gives the main mineral composition as described in Table 1.

The samples are prepared with the recommended water–grout (W/G) ratio. The recommended W/G are 1.7–3.1, 2.1 and 2.9–3.3 for Grout 1, Grout 2 and Grout 3, respectively (with the values used in the tests reported in Table 3). In addition, the particle densities are 2.76 gr/cm^3, 2.67 gr/cm^3 and 2.76 gr/cm^3 for Grout 1, Grout 2 and Grout 3. A variation of Grout 1 is also made to enhance the flowability and increase stiffness. To achieve this, the W/G ratio is increased to 2.8, and silica sand (solid density of 2.60 gr/cm^3) with a particle size distribution of 500–1000 μm and grout–sand ratio of 1.32

Table 1 Mineralogical analysis of grouts and clay pellets using XRD

Composition	G 1 [%]	G 2 [%]	G 3 [%]	CP 1 [%]	CP 2 [%]	CP 3 [%]
Quartz	8	23	16	29	28	16
Clay minerals	30	37	28	71	67	69
Cementation minerals	33	0	24	0	0	0
Graphite	0	40	0	0	0	0
Calcite	29	0	32	0	0	15
Magnetite	0	0	0	0	5	0

G = grout; CP = clay pellet

is added (Grout 1-S1). It has been shown that adding silica sand to the grout can cause plastic hardening behaviour, making the material stiffer (Erol and François 2013). The mineralogical analysis showed that Grout 1 has the highest concentration of cementation minerals, which generally leads to higher strength. In contrast, Grout 2 contains graphite to improve the thermal conductivity. Grout 3 contains a similar mineral composition to Grout 1, but the concentrations differ, with a lower percentage of cementation minerals.

Clay pellets

The 3 clay pellets used are available commercially and were provided by the suppliers with their permission for testing. They are commonly used materials for shallow ATES and groundwater wells. The clay pellets have the chemical composition as described in Table 1. It is highlighted that clay pellet 2 contains magnetite, which is used to allow the detection of annular materials via well logging. According to the suppliers specifications, clay pellet 1 and clay pellet 2 are Ca-bentonite clay pellets, whereas clay pellet 3 is a Na-bentonite clay pellet. Clay pellet 3 contains more than 60% smectite. The XRD measurements that are described in Table 1 are performed on bulk untreated powders and thus the smectite content is suppressed and does not appear explicitly in the XRD patterns (Deon et al 2022) but is included in the total clay content. Table 2 shows the physical and thermal properties of the clay pellets, with the pellet dimensions, water content and densities reported prior to hydration, and the thermal conductivities are for the hydrated pellet material.

Tables 1 and 2 show that mineralogical composition, physical and thermal properties are within the same range. However, differences in water content, particle density, and packing fraction are observed, which are critical variables for swelling and sealing behaviour. The main difference between the clay pellets is that clay pellet 3 is Na-bentonite, whereas clay pellets 1 and 2 are Ca-bentonite. This difference influences swelling capacity, since Na-bentonite clay pellets exhibit greater swelling capacity (Dananaj et al 2005).

Characterisation of the backfill material properties

The thermal and mechanical properties of the grouts were evaluated using standard methods for rock and concrete samples. Contrarily, the same procedures cannot be applied to the clay pellets because of the inhomogeneous mixture and plastic behaviour.

Thermal properties

The thermal conductivity (*k)* was determined using the transient plane source method (Hot Disk TPS2200). The grouts were tested in fully saturated conditions after curing

Table 2 Physical and thermal properties of the clay pellets

Clay pellet	L [mm]	D [mm]	WC [%]	k [W/mK]	ρ_p [g/cm^3]	ρ_b [g/cm^3]	η [-]
CP1	7–12	8	12.77	0.76	2.46	1.02	0.41
CP2	7–12	8	9.11	0.71	2.74	1.2	0.44
CP3	5–20	7–9	5.50	0.77	2.36	1.07	0.45

L = length; D = diameter; WC = water content; ρ_p = particle density; ρ_b = dry bulk density; η = packing fraction, k = thermal conductivity

Table 3 Grout mechanical and thermal properties for 7 and 28 curing period

Grout	W/G	G/S	Sand [mm]	7 days			28 days				
				UCS	σ_t	*E*	UCS	σ_t	*E*	ρ	*k*
				[MPa]	[MPa]	[GPa]	[MPa]	[MPa]	[GPa]	[kg/m^3]	[W/mK]
Grout 1	2.00	-	-	0.66	0.26	0.10	3.24	0.47	0.64	1289	0.81
Grout 2	2.16	-	-	0.36	0.11	0.16	1.51	0.31	0.54	1223	1.70
Grout 3	3.30	-	-	0.25	0.156	0.035	0.59	0.25	0.12	1200	0.73
Grout 1-S1	2.80	1.32	0.50–1.00	-	-	-	1.95	0.46	0.30	1323	0.86

The measured density corresponds to the saturated bulk density of the grout. G/S = grout–sand ratio

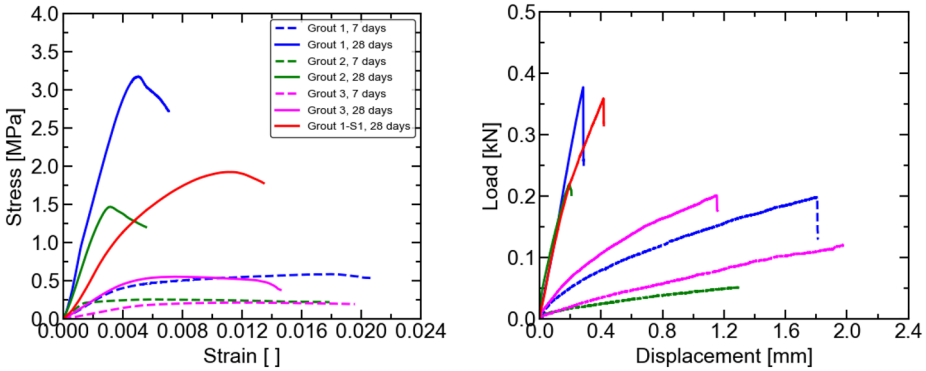

Fig. 2 Stress–strain and load–displacement data for the grouting materials for **a** UCS test; **b** Brazilian test

for 28 days, with the results shown in Table 3. Similarly, the clay pellets were tested in the hydrated state as shown in Table 2.

Uniaxial compressive strength and tensile strength

During the heating and cooling cycles, the grout was subjected to a large variation of stress due to the expansion and contraction of the tubing material and the grout itself. The uniaxial compression and tensile tests aimed to obtain the mechanical properties of the grout samples. The materials were tested after curing periods of 7 and 28 days, following the ASTM testing standards (ASTM D7012-14 2014; ASTM D3967-23 2023). The samples were submerged under water during the curing process, under a constant temperature of 22^{o}C, to ensure cement hydration and reduce the effects of curing in dry conditions, including thermal cracking and shrinkage. The Brazilian splitting test was used to determine the tensile strength (σ_t) and the uniaxial compressive strength (UCS) test was used to determine the Young's modulus (E), the UCS and qualitative information on the yield and failure process. These are shown for both the 7 and 28 days curing period in Figure 2, with a summary of results presented in Table 3. The variant of Grout 1, with increased W/G ratio and added silica sand (Grout 1-S1), was tested only for 28 days of curing.

The stress–strain relationship shows that for the 7 days curing period, the samples have low stiffness and strength and significantly deform after reaching the maximum stress, which corresponds to ductile material behaviour. This phenomenon can be

observed for both tests. In particular, it is observed that the sample behaves as an ideal plastic material (Figure 2a). After 28 days of curing, the peak stress and stiffness increase significantly for Grout 1 and 2, with Grout 3 showing the lowest strength and stiffness among the tested samples. Additionally, by increasing the W/G ratio for Grout 1-S1 and by adding 500–1000 μm sand particles to, the UCS reduced yet the tensile strength remained the same.

1-D free swell tests

A conventional 1-D free swell test apparatus is used to measure the free swelling of the clay pellets. The grouts are not tested as they do not exhibit swelling behaviour. The moisture contents after drying were 12.77 %, 9.11%, and 5.50 %, respectively. The tests are performed with fresh water and 0.25 mol/L NaCl to observe the effect of salinity on the swelling. This concentration is representative of brackish water. The granular clay pellets are placed in the cell after being dried in a 100^{o}C oven for two days. A vertical stress of 1 kPa is applied, with the material confined in the lateral direction by the chamber's walls. As the granular clay pellets saturate, the volume increases until it reaches a maximum saturation level. Figure 3a shows that clay pellet 3 exhibits the highest swelling, clay pellet 2 being the lowest and clay pellet 1 exhibiting intermediate behaviour. The higher swelling capacity of clay pellet 3 is predominantly due to the Na-bentonite composition, which has a significantly greater swelling potential than Ca-bentonite (Madsen and Müller-Vonmoos 1989). As observed in Figure 3b, by conducting the same experiments but with 0.25 mol/L NaCl, the swelling capacity decreases. The ratio of the final vertical swell with 0.25 mol/L NaCl relative to fresh water was approximately 0.28, 0.15 and 0.36 for clay pellet 1, clay pellet 2 and clay pellet 3, respectively. The higher swelling capacity of clay pellet 3 is predominantly due to the Na-bentonite composition.

Experimental procedure to quantify backfilling material hydraulic conductivity

Testing apparatus and procedure

Design of the apparatus

An apparatus is designed to simulate field conditions to reliably evaluate the sealing capacity of the annular materials (grouts and clay pellets). The design consists of the main apparatus, a data acquisition device (DAQ), a temperature controller, and a syringe pump, as illustrated in Figure 4. The outer part of the apparatus was thermally insulated

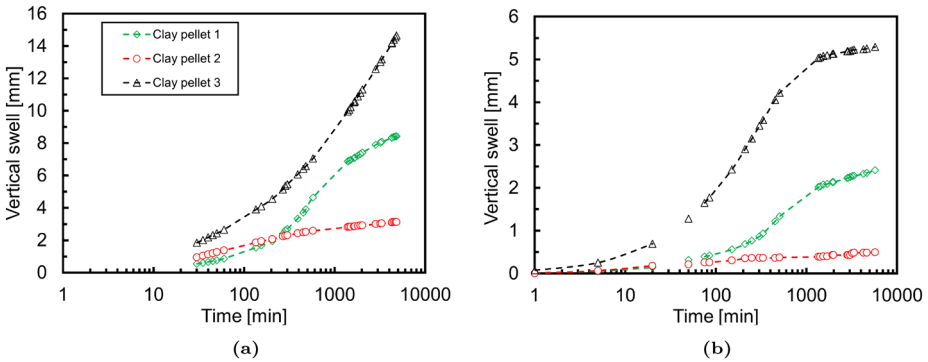

Fig. 3 1D free swell test with **a** fresh water and **b** 0.25 mol/L NaCl

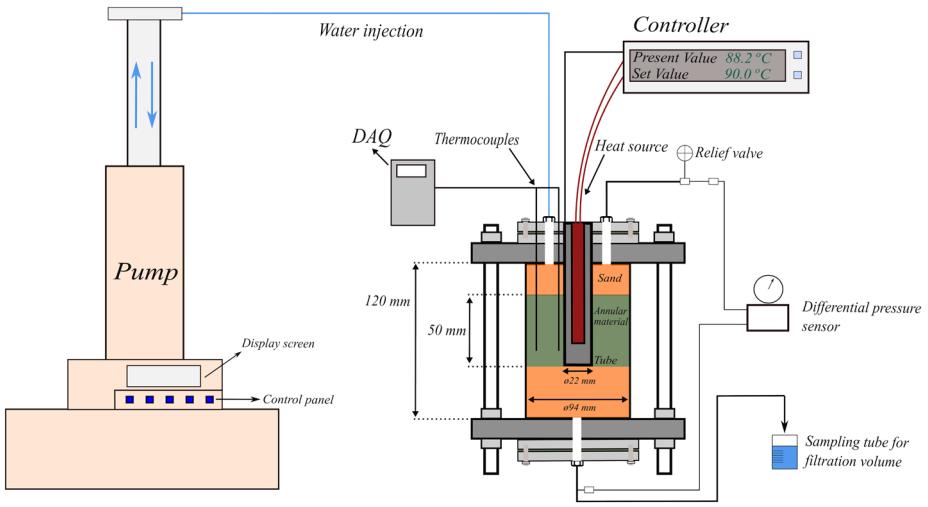

Fig. 4 Design of the experimental apparatus

with a foam sheet and a flame-retardant calcium-magnesium silicate thermal insulating sheet.

In the main apparatus, a sample of the sealing material was installed in a plexiglass cylinder around a model well-casing made of an aluminium tube, which includes a heating element (heat source) mounted in place with a thermal paste. A sand layer was below and above the sealing material in order to ensure equal water pressures above and below the sealing material and to investigate whether sand can migrate into any gaps in the sealing material. The plexiglass cylinder was mounted between two steel plates connected by steel rods and rubber gaskets to provide sealing. This provides vertical restraint in the experiment and ensures that the system is sealed. Ports are added at the top and bottom of the sealing plates to induce a flow in the sealing material or the interface between the aluminium tube and sealing material by injecting water at the top via the syringe pump and allowing free drainage at the bottom.

The apparatus contains three thermocouples which were used to control the temperature of the heating element (P1) and measure the spatial variation of the temperature at a distance of approximately 1.5 cm (P2) and 3 cm (P3) from the aluminium tube. A differential pressure sensor was installed and connected to the ports at the top and the bottom of the apparatus to enable the transmissivity to be calculated. The following aspects were considered during the design of the setup in order to be able to evaluate the performance of sealing materials:

- Aluminium is selected as a tube material instead of stainless steel to enable imaging via a micro-CT, as it reduces the scattering of the X-rays, thus, greater resolution across the interface area (see Section 3.3).
- Sand is placed as a top layer to observe if any sand particles were mobilised between the tube and the sealing materials.
- The frame of the apparatus is made of stainless steel, but is designed so that it can be disassembled with only the cylindrical plexiglass component entering the micro-CT scanner.

- The heating element is placed at the bottom of the tube, to observe if heating induces any differences in the sealing capacity.

Sample preparation procedure

In order to facilitate reliable and repeatable experiments, the following sample preparation procedure was followed for the grouts:

- The lowest part of the main apparatus was filled with gravel to a height of 1 cm to support uniform flow and prevent clogging.
- Unsaturated sand was compacted in place to a height of 5 cm.
- The sand was saturated from below to expel air from the system.
- The intermixture of grout with water was stirred to obtain the best possible homogeneous and consistent mass without lumps.
- The mixture (liquid form) was cast in the apparatus and has a height of approximately 5 cm.
- The upper cap of the apparatus was then installed in place to ensure a uniform hydration and sealing process of the grout with the centralised tube and thermocouples.
- Unsaturated sand is then added above the sealing material (without removing the upper cap, sand was slowly added through the connection using a funnel) and saturated with the syringe pump. During the saturation, the relief valve is opened to allow air to escape.

For the clay pellets experiments, the sample preparation procedure is practically similar. The main key difference was that the clay pellets were placed in the apparatus with a limited amount of water, ensuring sufficient water contact for swelling. Then, additional water was added to ensure the saturation of the clay pellets. Similarly, the saturation process was undertaken in the apparatus. In contrast to the grout tests, unsaturated sand was not added in the experiments with clay pellets. As the swelling progressed, the clay pellets occupied the entire available volume, leaving no available space.

Curing of the tested materials

The curing process is required to take place inside the main apparatus for the experiments conducted with grouts and clay pellets to investigate and evaluate the sealing capacity of the materials. At shallow depths, e.g. under 200 m, the temperature is a few degrees above the average surface temperature. For example, in the Netherlands, at a depth of approximately 150 m, the temperature is approximately 15^oC, therefore curing is undertaken at laboratory temperature ($\approx 22^oC$). The grout samples are left for the required period of time for curing (7 or 28 days). The clay pellets are saturated with water for 3 days before the thermal cycles.

Thermal cycle loading

The test is designed to mimic field operations, where hot water is injected or extracted via the wells as needed. Cycles are typically short-term during injection and extraction periods (summer and winter) and longer-term during periods where storage is not

needed to be charged or discharged (spring and fall). During the short-term cycles, the temperature at the borehole wall rises quickly to the injection temperature, with a temperature gradient through the grout due to the dominant heat transfer process of conduction. As the cycles are short, the temperature will not return to ambient conditions. In longer periods of inactivity, the temperature will reduce to almost ambient. The test procedure considers both of these heating cycles and is undertaken as follows, with the records of the test of Grout 3 shown in Figure 5 to demonstrate the procedure:

- The controller regulates the heating element temperature and is switched on with a target temperature of 90^{o}C, controlled via the inner thermocouple (P1). It continuously monitors the temperature acquired from the thermocouple (P1) and adjusts the power supplied to the heating element to maintain the desired temperature. The time depends on the grouting/pellets' thermal properties and thermal losses in the system.
- The inner thermocouple (P2) can reach temperatures up to 80^{o}C and the outer (P3) approximately 60–65^{o}C. Thus, during the experiments, once the outer thermocouple reached 60^{o}C, it was considered a steady state. Thus, the duration of the cycles was not fixed and can vary due to the temperature constraint and the manual adjustment required on the controller.
- The controller is adjusted to a lower setpoint, allowing the system to cool down naturally until the P1 temperature is approximately 40^{o}C.
- The above two stages are repeated until the number of short-term cycles has been achieved.
- The power was then remained off and the temperature was allowed to dissipate until approximately laboratory temperature.
- The integrity of the interface was then evaluated by performing injectivity tests (IT) to measure transmissivity. The syringe pump circulates fresh water or water with 0.25 mol/L NaCl with a constant flow rate (10 mL/min in all but one case, where it was 100 mL/min) while measuring the differential pressure across the sample and the outflow volume.
- The whole procedure was repeated as necessary.

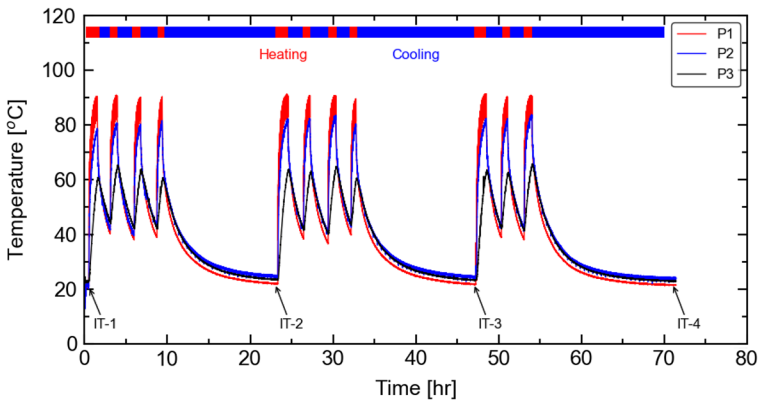

Fig. 5 An example of thermal cycles during testing of Grout 3, with measurements of the temperature distribution at the borehole wall (P1), and 1.50 cm (P2) and 3.00 cm (P3) distances from the centre of the tube

- The apparatus is disassembled and the plexiglass cylindrical component containing the sample was prepared for micro-CT which was performed after approximately 10–15 minutes.

Determination of hydraulic conductivity and transmissivity

Hydraulic conductivity and transmissivity are key properties which describe a material or system's (e.g. an aquifer) ability to transmit water. Hydraulic conductivity is a combined material and fluid property, whereas transmissivity includes also the system geometry, i.e. it is the product of the hydraulic conductivity and a length scale perpendicular to the flow direction, i.e. the aquifer thickness in aquifer systems as shown in Figure 6 and expressed mathematically as:

$$T = K_{av} b, \tag{1}$$

where T is the transmissivity (m^2/day), b is a length perpendicular to the flow, e.g. the aquifer thickness (m) and K_{av} is the average hydraulic conductivity (m/day). Transmissivity is often used in fractured systems or systems with inhomogeneities where the detailed material properties or geometry are hard to determine.

In a homogeneous medium, the hydraulic conductivity can be determined by obtaining/measuring the parameters described below:

$$K = \frac{Q\Delta L}{A\Delta H}, \tag{2}$$

where K is the hydraulic conductivity (m/day), Q is the flow rate (m^3/s), ΔL is the length in the direction of the flow which is considered (m), A is the area of the sample (m^2) and ΔH is the head difference (m) across the length. Figure 6 demonstrates the horizontal flow in a homogeneous aquifer with the hydraulic conductivity uniform and constant at any point.

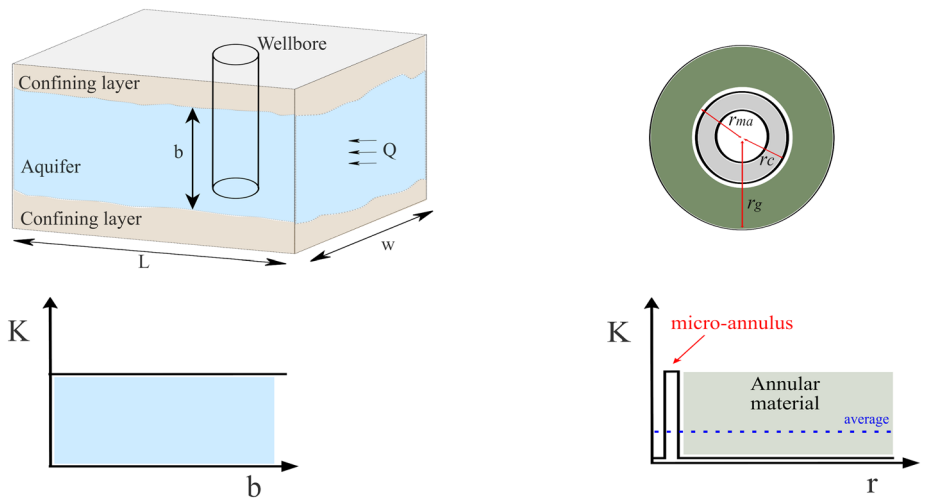

Fig. 6 Illustration of aquifer model (left) and cross-sectional well design showing casing, annular material, and micro-annulus (right)

The transmissivity can equally be calculated, but without the use of the cross-sectional area, rather a length in the second perpendicular direction to the flow (a direction where it is assumed the properties are uniform), i.e. the aquifer width (w) or the circumference of the grout or micro-annulus (C), e.g.:

$$T = \frac{Q\Delta L}{w\Delta H}. \tag{3}$$

As it is considered that a micro-annulus may be formed around the wellbore, as shown on the right-hand side of Figure 6, the flow would be unevenly distributed radially in the annular space, and measurements would no longer reflect the intrinsic property of the annular material.

Therefore, to be able to translate laboratory outcomes to field conditions, apparent transmissivity is used in the results, with the casing circumference used in Eq. 3 where a micro-annulus is assumed to occur.

To translate to an equivalent hydraulic conductivity, the appropriate length in the direction perpendicular to the flow is the annular thickness, i.e. the difference between the radius of the grout and the casing radius $r_g - r_c$. This is further used to translate from laboratory and field conditions later in the paper.

Imaging

Micro-computed tomography (micro-CT) was utilised to characterise the samples, using a TESCAN, CoreTOM Micro-CT. The samples were scanned with a resolution of 100 μm, and the area of interest was the interface between the tube and annular material. Due to the large size of the testing apparatus, the resolution was limited to 100 μm to allow scanning of the entire tube length. This resolution represents a limitation, as fine features below 100 μm cannot be detected. The resulting cross-sectional images are a series of multiple scans of the sample. The images were processed in the following manner to quantify and visualise any resulting gaps (micro-annulus) between the sealing material and the tube.

The distance between the base (sample location) and the X-ray source was adjustable and deviated for each sample. Thus, each sample's region of interest (ROI) was slightly different. The acquired files contained relative information about each scan, including resolution, scanning time and voxel size. VGStudio Max was utilised for the image processing. The files were imported as an image stack with the appropriate voxel size, which is utilised to recalibrate the pixel to the actual size during the reconstruction process. An artificial volume was created across the interface to reduce the noise's effect and improve the reconstruction's quality. By adjusting the tolerance and the threshold colour in the region of interest, the area with similar intensity and density was selected. In several cases, the parts with similar intensity were not connected, and thus this process is re-applied by selecting manually the part of interest. To visualise the volume, the pixels of interest were extracted and highlighted with a yellow colour and exported in DICOM format as individual slices. The calculated interface area reflects an irregular geometry rather than a circle, capturing the order of magnitude for each slice accurately.

Results

Grouts curing period—7 days

Thermal cycling loading induces deformation across the interface and the formation of a micro-annulus, resulting in a preferential path for water to flow, as detailed further below. In general, the tested grouts are low-strength and low-stiffness materials; However, differences in their mineral composition had an effect on their response to thermal cycles. shows poor bonding at the interface, Grout 2 exhibits permanent deformation under thermal cyclic loading. However, Grout 3, which contained a higher percentage of quartz and calcite, showed significantly lower deformation.

During the injectivity tests (IT) undertaken with 100 mL/min, water was injected from the upper part of the apparatus with differential pressure and outflow volume was measured. To minimise the risk of artificially inducing flow paths, the differential pressure was restricted to a maximum of 1000 mbar. Consequently, steady-state conditions were not achieved for several tests. In these cases, transmissivity was estimated using the maximum recorded differential pressure and the outflow volume, which in several tests differs from the inflow. This approach results in an underestimation (lower limit) of transmissivity values, with the actual transmissivity being larger than reported. Therefore, we refer to it as apparent transmissivity. However, relative transmissivities can be compared. For tests in which steady-state conditions were achieved, the apparent transmissivity is equal to the actual transmissivity.

The results obtained from the experiments conducted show that the apparent transmissivity evolves with heating and cooling cycles, as shown in Figure 7. Grout 1 is seen to have a low differential pressure, indicating a low resistance to flow, which reduces slightly with thermal cycles. In addition, the results indicate that the initial curing suggests poor bonding around the tube, due to the steady-state differential pressure in the IT-1 (Figure 7). It is observed for Grout 2 that during the first 3 injection tests, the differential pressure rises throughout the test, reaching around 500 mbar after around 60 seconds. During the 4th injectivity test (IT-4), the angle of the slope of differential pressure is lower, indicating less resistance across the interface and the sample. The 5th injectivity test (IT-5) results indicated a compromise of the interface area with an almost negligible pressure during the test. In contrast, Grout 3 showed relatively similar pressure build-ups during all injectivity tests.

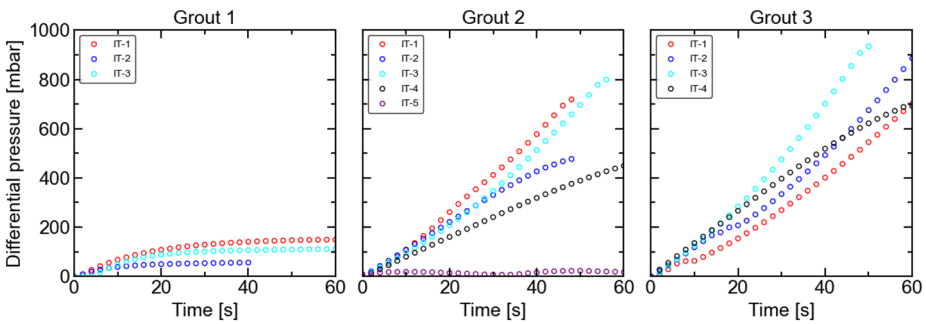

Fig. 7 Measured differential pressure across the samples during the injectivity tests (IT) at ambient temperature. The differential pressure is normalised such that the initial value is set to zero

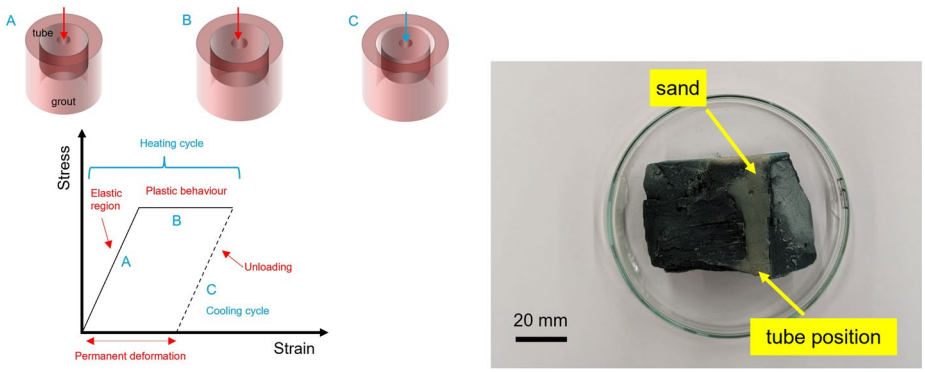

(a) (b)

Fig. 8 **a** Graphical illustration of the effect of heating and cooling cycles on plastic grouts; **b** extracted material after the Grout 1 experiment

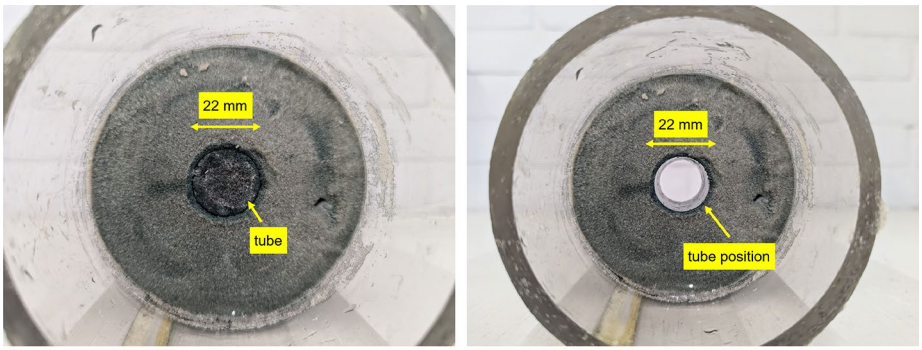

(a) (b)

Fig. 9 Grout 1 experiment with a reduced flow rate. Bottom view photos obtained after the test **a** before and **b** after removing the tube

In Grout 1, the initial test that was performed with 100 mL/min, as opposed to the other samples of 10 mL/min, sand was detected in the micro-annulus, as shown in Figure 8b. This is considered to occur due to plastic deformation of the grout during the heating and cooling cycles and poor initial bonding at the interface. It is important to state that poor bonding alone does not result in sand mobilisation. The sand has particle diameters between 175 and 250 μm, meaning that additional deformation beyond the initial bond failure is required for particles to enter the interface. In contrast, the tube suffers elastic deformation, as shown in Figure 8a. Due to the plastic behaviour of the sample, while the apparatus cools down, the sample does not return to its original state, allowing the sand from the upper layer to enter the interface (Figure 8b). This phenomenon is not observed in the outer layer of the grout.

An additional experiment was performed under the same conditions, but during the injectivity test the injection rate was reduced to 10 mL/min. Figure 9a presents an image of the lower part of the apparatus after the sand section is removed and indicates a clear space between the grout and the tube, indicating that the interface has been compromised similarly. However, Figure 9b shows that no sand particles entered the interface. This indicates that the higher the injection flow rate, the higher the effect on mobilising sand particles. In both cases, the high moisture content in the interface after removing

the tube indicates a flow path during the injectivity tests. Compared to Grout 2, where the heating and cooling cycles have a clear effect, the behaviour observed in Grout 1 results from the combined influence of poor initial bonding and the thermal cycling.

Compared with Grout 1 and 3, Grout 2 has significantly higher thermal conductivity (see Table 3), which reduces the thermal gradient and distributes the temperature changes more evenly throughout the sample. However, under 7 days of curing, the sample has relatively low stiffness corresponding to limited resistance to thermal stress. The images obtained from the micro-CT scan (Figure 10a) show a deformation around the interface between the tube and the grout.

A three-dimensional view and the calculated interface area (the micro-annulus cross-sectional area) along the tube length after the test are presented in Figure 11 for Grout 2. This demonstrates that the deformation across the length of the grouting material coincides with where the heating element was located. Since the heating element was not in contact with the tube's lower part, the temperature changes are lower than in the upper part. Thus, the heating and cooling cycles are less severe, leading to less deformation. The plastic deformation of the grouting material is greater in the top part of the tubing (where the heating element is placed).

The interface areas occurrences are shown for Grouts 2 and 3 in Figure 12, for the zones with and without the heating element. The data show that in the zone with a heating element (HE), the increase in the interface area is significantly higher for both cases. Subsequently, Grout 3 exhibited significantly more resilience during the heating and cooling cycles, supporting the results of the injectivity tests.

By including data of the outflow water, the apparent transmissivity in the injectivity tests can be calculated (Figure 13). Only the tests which result in a steady differential pressure can be considered to be measurements of the actual transmissivity, but the final values of differential pressure are used to calculate a value which is useful for

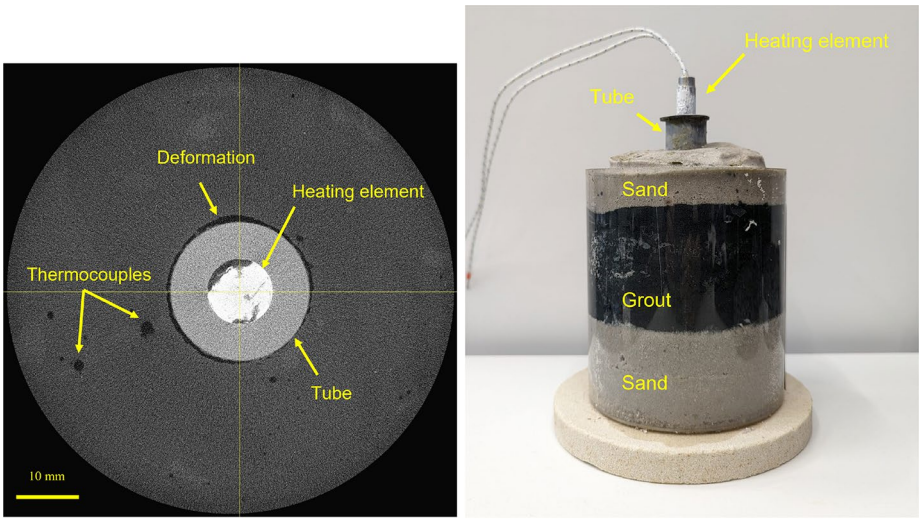

Fig. 10 Photos obtained after testing of Grout 2. **a** Top view after the image reconstruction; **b** illustration of disassembled apparatus before the micro-CT scan

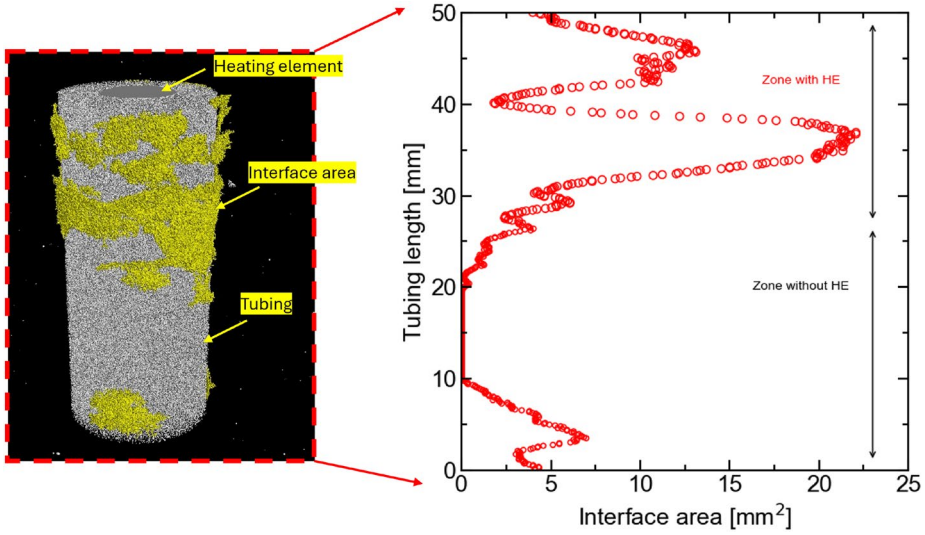

Fig. 11 3D view after the image reconstruction of Grout 2. Interface area as a function of tube length. Note* HE = heating element

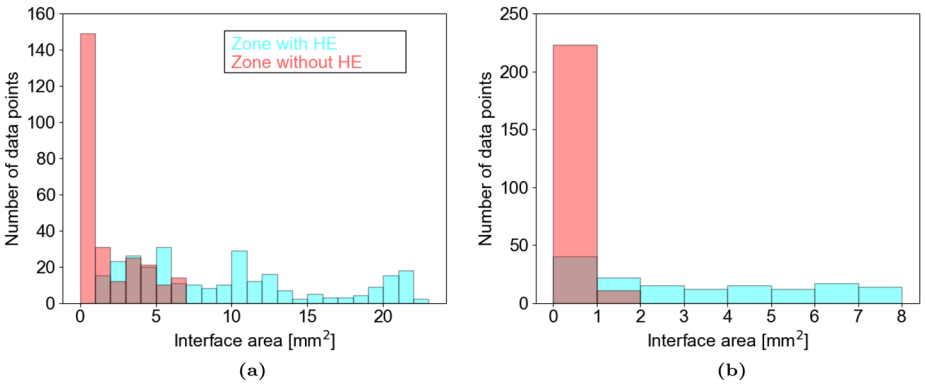

Fig. 12 The total number of data points at each interface area zone (with or without heating element): **a** Grout 2; **b** Grout 3

comparison. The initial apparent transmissivity, which is associated with conditions where there was a bond between the tube and the grout, is used as a benchmark and generally shows the lowest value. Injectivity test 4 was not performed on Grout 1, while injectivity test 5 was only performed for Grout 2.

Grouts curing period—28 days

Tests were performed on samples cured for 28 days. Micro-CT scans revealed a significant decrease in the size of the interface area for Grouts 1 and 2 (see Figure 14), which corresponds to lower apparent transmissivity values. On the other hand, Grout 3 showed an increase in the interface area, leading to higher apparent transmissivity compared to the performance during 7 days of curing. The sample containing silica sand (Grout 1-S1) showed the largest increase in the interface area and the highest apparent transmissivity in all samples, indicating poor long-term integrity.

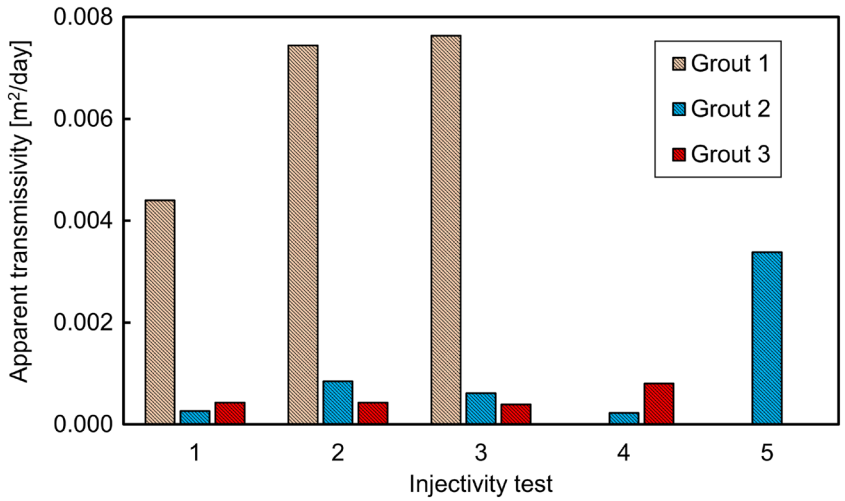

Fig. 13 Injectivity tests to measure the apparent transmissivity after a specific number of cycles

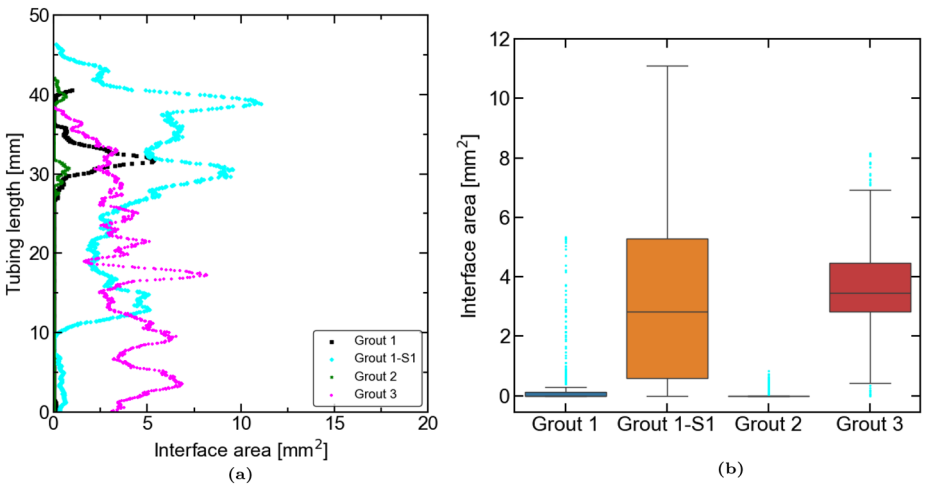

Fig. 14 **a** Interface area as a function of tube length; **b** boxplot representation of the distribution for the entire data set

As with the analysis during the 7 days, a 3D reconstruction of the tested samples was conducted to measure the interface area. Figure 15 shows the increase in the interface area as a function of tubing length for Grout 3. The results indicate an increase across this zone.

Interestingly, the Grout 3 shows a compromise in the interface, even though the 7 days cured sample demonstrated an impermeable interface. The curing process and laboratory temperature are identical to the previous samples. As observed from the mechanical tests (Figure 2), Grout 3 showed a minor gradual increase in strength and stiffness over different curing periods.

Grout 1-S1 containing sand particles shows the largest variation and local increase in the interface area (Figure 14a). A partial contribution to this result is the greater W/G ratio. Even though Grout 2 and Grout 1-S1 have similar UCS, the Young's

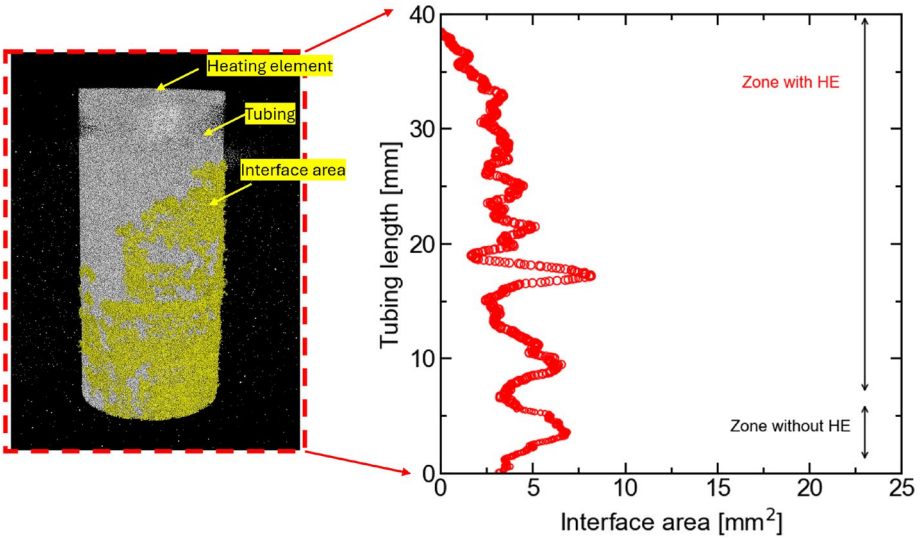

Fig. 15 3D view after the image reconstruction of Grout 3 and interface area as a function of tube length. Note* HE stands for the heating element

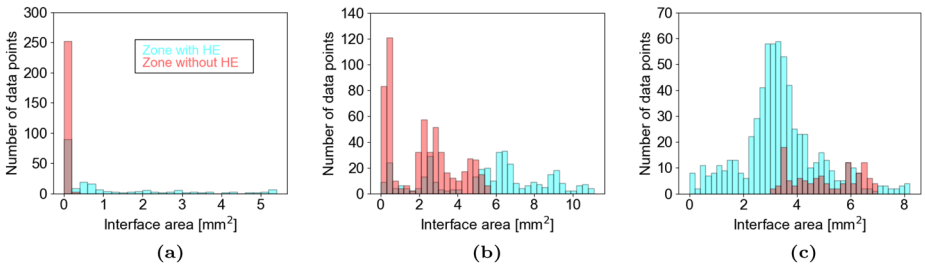

Fig. 16 Distribution of increase in interface area for zones with and without heating element: **a** Grout 1; **b** Grout 1-S1; **c** Grout 3

modulus (E) is considerably higher for Grout 2 and Grout 3 shows non-linearity in the UCS, indicating the likelihood of earlier plastic deformation. The distribution of the entire data set is summarised in Figure 14b, with Grout 1 and Grout 2 having the lowest median line. Grout 1-S1 exhibits the highest variability with local increases, whereas Grout 3 displays an increase in the interface area across the tube's length.

Figure 16 shows the increase in interface area for Grouts 1, 1-S1 and 3. Grout 2 is not shown due to the almost negligible increase which was below the detection limit of 100 μm resolution. The increase in the interface area is significantly lower for the zone without a heating element (HE). Similar to Grout 2, Grout 1 showed an excellent sealing capacity with only a limited form of micro-annulus detectable with the current resolution. Grout 1-S1 exhibited a spread of deformation in both areas, with and without the heating element, with the highest deformations concentrated in the zone with the heating element. In Grout 3, significant deformation occurred in the zone with a heating element, which varied along the length. Consequently, an increase in the interface area below this resolution was not captured, with the possibility of having a preferential flow path.

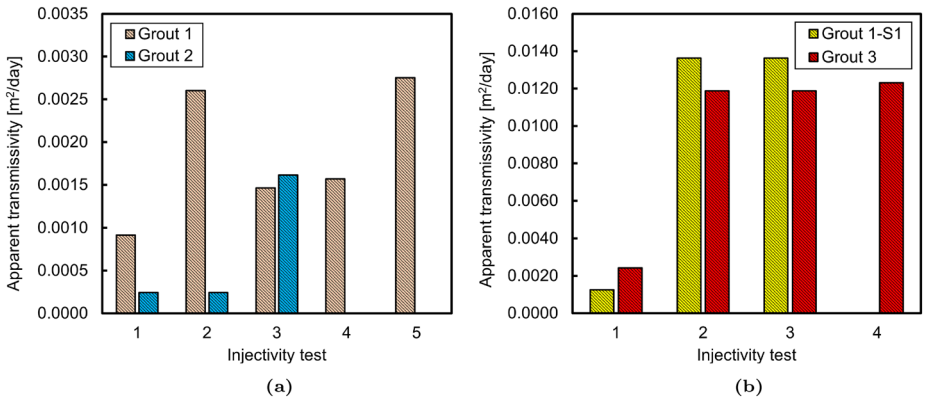

Fig. 17 Apparent transmissivity derived from the injectivity tests performed at a 10 mL/min flow rate on samples cured for 28 days

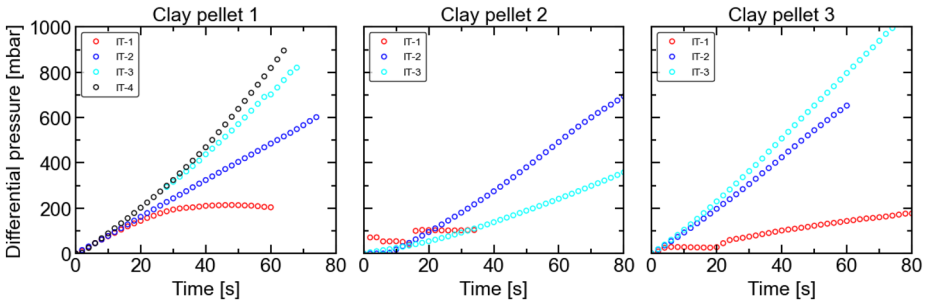

Fig. 18 Measured differential pressure across the clay pellets during the injectivity tests (IT) at ambient temperature

Figure 17 demonstrates that the corresponding apparent transmissivity for Grout 1 and 2 has decreased compared to the injectivity tests that were performed on the grouts within 7 days of curing, but still increased during thermal cycles. Grouts 1-S1 and 3 are seen to have a significantly higher apparent transmissivity.

The micro-CT scans for Grout 1 and 2 indicated that the interface is mostly intact, within the resolution limits. Thus, any fine features or discontinuities below 100 μm may not be clearly visible in the micro-CT images, yet they can act as flow paths. Consequently, it causes the corresponding low apparent transmissivity during the injectivity tests. However, there was a relative increase in apparent transmissivity values during the injectivity tests, indicating some degradation of the interface.

Clay pellets

Clay pellets absorb water to swell, and the pore structure of the mixture reduces as a function of time. The evolution of the increased swelling capacity has resulted in a significant increase in the sealing performance of the annular space as a function of time. The impact of the impermeable behaviour of the clay pellets can be observed with the pressure build-up during the injectivity tests in Figure 18. In the initial injectivity test (IT-1), outflow was measured for clay pellets 1 and 2, which can also be correlated with the steady pressure after approximately 30 and 20 seconds, respectively. The subsequent

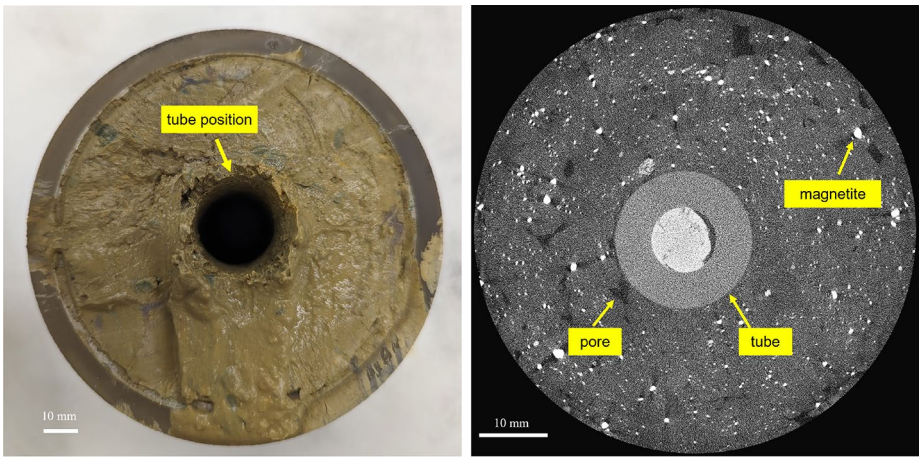

Fig. 19 Optical and micro-CT images of clay pellets after thermal cycles. **a** Clay pellet 1, having removed the inner tube, showing the homogeneous mixture with no visible pores; **b** clay pellet 2 micro-CT scan image indicating isolated pores

Table 4 Apparent transmissivity for the clay pellets based on injectivity tests

Material	IT-1 Apparent T [m^2/d]	IT-2 Apparent T [m^2/d]	IT-3 Apparent T [m^2/d]	IT-4 Apparent T [m^2/d]
Clay pellet 1	5.11E-03	1.76E-04	6.39E-06	5.08E-06
Clay pellet 2	6.22E-05	6.20E-06	5.08E-06	-
Clay pellet 3	5.11E-03	5.99E-05	1.24E-05	-
Clay pellet 1, 0.25 NaCl	1.88E-03	3.10E-04	2.92E-04	3.83E-05
Clay pellet 2, 0.25 NaCl	1.02E-03	8.46E-04	9.06E-04	6.67E-04
Clay pellet 3, 0.25 NaCl	4.03E-05	4.96E-06	5.74E-06	1.36E-06

injectivity tests demonstrated a pressure build-up to 900 mbar, with similar behaviour observed for clay pellet 3. The sealing performance for clay pellets was improved as a function of the thermal cycles, suggesting an additional saturation of the pellets during this time. However, the slower pressure build-up for clay pellet 2 correlates with the smaller volume increase during the 1D free swell tests.

Figure 19 shows the homogeneous filling of the annulus by clay pellets 1 and 2 after thermal cycling. The micro-CT scan image (Figure 19b) shows that the clay pellets are resilient to thermal cycles when hydrated with fresh water. In Figure 19b, the micro-CT scans reveal isolated pores and the absence of a micro-annulus; However, features below the resolution limit cannot be excluded. Figure 19a shows that clay pellets are a homogeneous mixture after saturation, achieving a low permeability barrier that provides effective sealing and minimises water migration.

All the experiments were also repeated with clay pellets saturated with water with 0.25 mol/L NaCl, as they showed low apparent transmissivity during the fresh water experiments. For tests where the outflow was limited or was not observed, it was assumed that the outflow volume was half of a droplet, corresponding to 0.025 mL. Table 4 shows

the calculated apparent transmissivity for the clay pellets during four injection tests (IT). The initial apparent transmissivity observed during IT-1, conducted prior to thermal cycles, is consistently higher for all clay pellets. Following the thermal cycling, the apparent transmissivity tends to decrease in subsequent tests for almost all clay pellets, except IT-2 and IT-3 for clay pellet 3. This reduction is caused by the increased interaction between the clay pellets and water, potentially leading to enhanced hydration and additional swelling, thereby reducing the overall apparent transmissivity as a function of time.

For the experiments conducted with 0.25 mol/L NaCl, clay pellets 1 and 3 showed lower apparent transmissivity compared to clay pellet 2. However, all clay pellets demonstrated higher overall apparent transmissivity for each test in comparison to the fresh water experiments. Clay pellet 1 and 3 were maintained for an extended period in the apparatus without applying thermal cycles to determine any changes in the apparent transmissivity. For clay pellet 1 the apparent transmissivity values obtained after 1 day and 5 days were $3.51E{-}5$ and $1.29E{-}5$ m^2/day, respectively. Similarly, for clay pellet 3 the apparent transmissivity value after 5 days was $7.10E{-}6$ m^2/day. These results indicated that the clay pellet continued to slowly hydrate over time.

Discussion

The work introduced an experimental framework to simulate the heating and cooling cycles and conduct quantitative analysis for backfilling material integrity, by measuring the apparent transmissivity and imaging using micro-CT. The formation of the micro-annulus is identified using image processing of the micro-CT scans and combined with injectivity tests to evaluate the sealing capacity. In the context of HT-ATES, the conditions of the shallow environment are similar, but the operating temperatures are significantly higher. The results indicate that for a 7 day curing period, the grouts show a plastic behaviour during the thermal cycles, with the tendency to deform plastically at the interface, resulting in the formation of the micro-annulus. Even though the amplitude of the thermal stress is lower at the bottom part of the tube (zone without heating element), a slight increase at the interface area is observed, suggesting a limited resilience to thermal cycles. Contrarily, for 28 days of curing, the grouts achieved higher strength and stiffness, with the resulting effect of thermal stress decreasing for 3 of the grouts.

The study aimed to replicate the relevant conditions for HT-ATES systems. In wells installed in the field, composite or stainless steel casings will be used rather than aluminium, corresponding to a lower thermal expansion coefficient. In practice this will result in a lower stress transfer to the grout due to expansion and contraction. Thus, the severity of the heating and cooling cycles using stainless steel is expected to be less for the 90^oC condition. In the lab tests, the temperature variation ranges from 22 to 90^oC. For the casing radius used in the experiments of $r_c = 11$ mm, the radial displacement Δr is 0.016 mm for aluminium. Considering the same conditions for stainless steel, the Δr would be 0.014 mm. Aluminium was therefore used to allow detection of the micro-annulus in the micro-CT, and to provide a conservative upper bound for the sealing integrity. However, we acknowledge that the resulting expansion may exceed what would occur in stainless steel casings. Therefore, our results are

likely to show an extreme case. Therefore, the maximum temperature with aluminium should have been slightly adjusted to be representative of a stainless steel casing under similar conditions.

The increase of the tube temperature during heating cycles to approximately 90^oC reflects the operational mode during the discharging of the HT-ATES. Similarly, the temperature in the well can be decreased to 40^oC during well rehabilitation. However, the temperature in the well and the surrounding soil returns to the initial ambient temperature when the system's operation is stopped. This scenario is demonstrated approximately 3 to 4 times during the current experimental framework's grout and clay-pellet test. Thus, the most significant impact on the interface area is a combination of annular material mechanical properties and the large temperature variation during the cooling cycle. These factors contribute to the annular material's mechanical behaviour and long-term sealing performance.

Even though Grout 2 demonstrates low apparent transmissivity values for 28 days of curing, the corresponding high thermal conductivity adds a challenge. HT-ATES lifespan and economic viability highly depend on the heat extraction. Heat transfer occurs between the tubing (casing), the annular material and the surrounding soil and is a function of the thermal properties. Consequently, in the case of Grout 2, the heat losses can be expected to be higher than any other grouting and clay-pellet materials tested in this study. Further research is needed to quantify the extent to which high thermal conductivity affects performance, as this is also affected by operation, depth, and geohydrological conditions.

Regarding the clay pellets, the initial free swell test showed that clay pellet 3 has a significantly higher swelling capacity compared to the other two tested samples. The results for clay pellets 1 and 3 show a limited initial apparent transmissivity before the heating and cooling cycles, which decreased in further tests. This may (partially) be explained by the fact that the saturation period was 3 days prior to the experiments. In field applications saturation of backfilling material is more likely to be weeks or even months before thermal stresses occur. Therefore, the initial transmissivity in the field can be expected to be lower than the initial values presented here. As it was stated, the current experimental approach underestimates the transmissivity values for both the clay pellets and grouts since a steady state was not reached during several injectivity tests. The current approach utilises the outflow volume which differs from the inflow; thus, we have reported the apparent transmissivity. For the same conditions, the actual transmissivity is expected to be higher.

Because no micro-annulus was observed in the experiments with the clay pellets, the apparent transmissivity is used to compute the hydraulic conductivities. For the fresh water experiments, clay pellets 1 and 2 achieved slightly better sealing capacity than clay pellets 3, which does not follow the expectation that higher swelling pressure would result in better sealing. After the first thermal cycles, all clay pellets sealed better. After several periods of thermal cycles and also consequently longer time in the setup, all clay pellets demonstrated a low apparent transmissivity, corresponding to a hydraulic conductivity in the annulus of 10^{-9} m/s. Following the additional experiments using water with a 0.25 mol/L NaCl concentration, clay pellets 1 and 3 achieved slightly increased apparent transmissivity values still corresponding to a

hydraulic conductivity of 10^{-9} m/s, with clay pellets 2 to be in the range of 10^{-8} m/s. For an additional 5 days, the clay pellets 1 and 3 remained at the setup, with testing values approximately at 10^{-10} m/s.

To evaluate whether the backfilling materials comply with regulations that specify the hydraulic conductivity ($< 10^{-9}$ m/s), the laboratory apparent transmissivities have been translated to average annular hydraulic conductivities in field conditions. The approach taken was to assume that the vast majority of the flow occurs in the micro-annulus caused by the thermal cycles. In addition, it was assumed that the micro-annulus has the same (average) radius as in the laboratory. The scaling was then undertaken by assuming that the apparent transmissivity was equal, and then it can be divided by the annular thickness to obtain a field average hydraulic conductivity. In the case of clay pellets, due to the absence of micro-annulus, the hydraulic conductivity achieved in the laboratory is expected to be similar in the field. Thus, upscaling is not required. The conventional diameter of the drill bit (well diameter) for the target depth is on the order of magnitude of 600 mm, and the casing diameter is approximately 300 mm. In the experiments, the sample diameter is 94 mm with a casing of 22 mm. One factor contributing to the field-scale hydraulic conductivity being larger compared to the laboratory measurements is the size of the casing and the material properties. Considering similar thermal conditions, the 300 mm stainless steel tube exhibits approximately 13 times greater linear expansion than the 22 mm tube. Another factor is the geometric difference in the ratio between the annulus (r_g) and tube/casing (r_c). By assuming the same apparent transmissivity in the laboratory and the field, the average hydraulic conductivity is:

$$K = \frac{T_{ap}C}{A}, \tag{4}$$

where A is the area of the annulus (m^2). This relationship allows for the interpretation of laboratory data for application in field-scale models, as geometric and boundary conditions can significantly impact the hydraulic properties. Based on the current experimental framework, it is concluded that $r_g >> r_{ma}$, where r_{ma} is the size of the micro-annulus. This expression can also be assumed for the field conditions. In Table 5, the estimated hydraulic conductivity in field conditions is presented for the grouts. The upscaling suggests that the grouts do not fulfil the specified hydraulic conductivity threshold, even though within a small margin. As it was mentioned, the laboratory analysis was conducted using an aluminium tube, whereas stainless steel would be used in the field. Hence, a lower hydraulic conductivity is expected under actual field conditions.

Table 5 Estimated average hydraulic conductivity field conditions

Well diameter [m]	Casing diameter [m]	Annulus area [m^2]	K (Grout 1) [m/s]	K (Grout 2) [m/s]	K (Grout 3) [m/s]
0.3	0.2	0.039	5.10E-07	2.99E-07	2.28E-06
0.6	0.3	0.212	1.42E-07	8.30E-08	6.33E-07
0.9	0.6	0.353	1.70E-07	9.96E-08	7.60E-07

To quantify the geometrical effects, future work should consider implementing actual casing and wellbore sizes. Thus, it reduces the influence of dimensions and enhances the prediction of the laboratory data.

Conclusions

The study investigated the sealing capacity of grout and clay pellet wellbore completion materials under heating and cooling cycles for shallow wells. The experimental demonstration combined with extensive image processing reveals and supports the evidence of the plastic deformation across the interface. The study contributes to the quantification of the sealing characteristics of annular materials for HT-ATES systems. The results are summarised in the following highlights:

- Plastic deformation was observed after thermal cycling, for grouts with low strength and stiffness.
- Image processing provides an insightful, revealing debonding and formation of micro-annuli.
- Apparent transmissivity decreased up to 80% for grout samples cured for 28 days, compared to 7 days curing.
- Higher concentrations of cementation additives ensure greater strength and stiffness.
- The formation of micro-annuli across the interface is substantial evidence of thermal expansion and plastic deformation, although features below the 100 μm cannot be excluded.
- For fresh water thermal cycles, the clay pellets showed impermeable behaviour, indicating an intact interface, within the resolution limits, and demonstrating resilience to thermal cycles.
- The experiments conducted with 0.25 mol/L NaCl showed a slower decline of apparent transmissivity values compared to the fresh water during the injectivity tests, but ultimately reached an impermeable behaviour.

Abbreviatons

CP	Clay pellet
G	Grout
HT-ATES	High-temperature aquifer thermal energy storage
HE	Heating element
IT	Injectivity test

Acknowledgements
The authors thank Arjan Thijssen and Ellen Meijvogel-de Koning for their help in performing the micro-CT scanning.

Author contributions
A.K: conceptualisation, methodology, formal analysis and investigation, writing—original draft preparation; M.B: funding acquisition, conceptualisation, methodology, supervision, contributed to writing—review and editing; P.V: conceptualisation, methodology, funding acquisition, supervision, contributed to writing—review and editing.

Funding
This work was funded by the European Union under the Horizon Europe programme (grant no. 1011096566). Views and opinions expressed are however those of the author(s) only and do not necessarily reflect those of the European Union or CINEA. Neither the European Union nor CINEA can be held responsible for them.

Data availability
No datasets were generated or analysed during the current study.

Declarations

Competing interests
The authors declare no competing interests.

Received: 28 October 2025 Accepted: 26 January 2026
Published online: 06 February 2026

References

ASTM D3967-23. International, standard test method for splitting tensile strength of intact rock core specimens with flat loading platens. American society for testing and materials. 2023.
ASTM D7012-14. Standard test methods for compressive strength and elastic moduli of intact rock core specimens under varying states of stress and temperatures. American Society for Testing and Materials. 2014.
Birdsell DT, Adams BM, Saar MO. Minimum transmissivity and optimal well spacing and flow rate for high-temperature aquifer thermal energy storage. Appl Energy. 2021;289:116658. https://doi.org/10.1016/j.apenergy.2021.116658.
Bloemendal M, Hartog N. Analysis of the impact of storage conditions on the thermal recovery efficiency of low-temperature ATES systems. Geothermics. 2018;71:306–19. https://doi.org/10.1016/j.geothermics.2017.10.009.
Bloemendal M, Vardon P, Medema A, Snelleman S, Marif K, Beernink S, Van Oort T. Feasibility study ht-ates at the tu delft campus. Delft University of Technology & ENGIE. 2020.
Bloemendal M, Vardon P, Pijnenborg M, Sudintas G, Medema A, Marif K, Beernink S, van Veldhuizen F, et al. A techno-economic evaluation of high temperature thermal aquifer storage (ht-ates) for use with the geothermal well on the tu delft campus. In: Proceedings World Geothermal Congress 2020. 2021.
Bois AP, Garnier A, Rodot F, Saint-Marc J, Aimard N, et al. How to prevent loss of zonal isolation through a comprehensive analysis of microannulus formation. SPE Drill Compl. 2011;26(01):13–31. https://doi.org/10.2118/124719-PA.
Bois AP, Garnier A, Galdiolo G, Laudet JB. Use of a mechanistic model to forecast cement-sheath integrity. SPE Drill Compl. 2012;27(02):303–14. https://doi.org/10.2118/139668-PA.
Dananaj I, Frankovská J, Janotka I. The influence of smectite content on microstructure and geotechnical properties of calcium and sodium bentonites. Appl Clay Sci. 2005;28(1–4):223–32.
Daniilidis A, Mindel JE, De Oliveira FF, Guglielmetti L. Techno-economic assessment and operational CO2 emissions of high-temperature aquifer thermal energy storage (HT-ATES) using demand-driven and subsurface-constrained dimensioning. Energy. 2022;249:123682. https://doi.org/10.1016/j.energy.2022.123682.
Darde B, Roux JN, Pereira JM, Dangla P, Talandier J, Vu MN, et al. Investigating the hydromechanical behaviour of bentonite pellets by swelling pressure tests and discrete element modelling. Acta Geotech. 2021;16:507–24. https://doi.org/10.1007/s11440-020-01040-5.
De Andrade J, Sangesland S, Todorovic J, Vrålstad T. Cement sheath integrity during thermal cycling: a novel approach for experimental tests of cement systems. In: SPE Norway Subsurface Conference. SPE. 2015: pp. SPE–173871. https://doi.org/10.2118/173871-MS
Deon F, van Ruitenbeek F, van der Werff H, van der Meijde M, Marcatelli C. Detection of interlayered illite/smectite clay minerals with XRD, SEM analyses and reflectance spectroscopy. Sensors. 2022;22(9):3602.
Dinkelman D, Bergen F. Evaluation of the country-wide potential for high-temperature aquifer thermal energy storage (ht-ates) in the Netherlands. 2022.
Dinkelman D, Carpentier S, Koenen M, Oerlemans P, Godschalk B, Peters E, Bos W, Vrijlandt M, et al. High-temperature aquifer thermal energy storage performance in middenmeer, the netherlands: thermal monitoring and model calibration. In: Proceedings of the European Geothermal Congress. 2022.
Erol S, François B. Thermal, hydraulic and mechanical performances of enhanced grouting materials for borehole heat exchanger. In: TC215 CPEG (Coupled Phenomena in Environmental Geotechnics) Symposium. Torino. 2013.
Fischer HR, Moghadam A. Testing various cement formulations under temperature cycles and drying shrinkage for low-temperature geothermal wells. Materials. 2023;16(23):7281. https://doi.org/10.3390/ma16237281.
Goodwin K, Crook R. Cement sheath stress failure. SPE Drill Eng. 1992;7(04):291–6.
Guerra AM, Aimedieu P, Bornert M, Cui YJ, Tang AM, Sun Z, et al. Analysis of the structural changes of a pellet/powder bentonite mixture upon wetting by x-ray computed microtomography. Appl Clay Sci. 2018;165:164–9. https://doi.org/10.1016/j.clay.2018.07.043.
Ichim A, Teodoriu HC. Investigations on the surface well cement integrity induced by thermal cycles considering an improved overall transfer coefficient. J Pet Sci Eng. 2017;154:479–87. https://doi.org/10.1016/j.petrol.2017.02.013.
Kiran R, Teodoriu C, Dadmohammadi Y, Nygaard R, Wood D, Mokhtari M, et al. Identification and evaluation of well integrity and causes of failure of well integrity barriers (a review). J Nat Gas Sci Eng. 2017;45:511–26. https://doi.org/10.1016/j.jngse.2017.05.009.
Laterlite. Expanded clay. 2025. https://www.laterlite.com/wp-content/uploads/2022/05/Technical-data-sheet-Laterlite-Expanded-Clay.pdf. Accessed 28 May 2025.
Lavrov A, Torsæter M, Lavrov A, Torsæter M. Thermal stresses in annular cement. Physics and mechanics of primary well cementing. 2016. p. 93–101. https://doi.org/10.1007/978-3-319-43165-9.
Lee C, Lee K, Choi H, Choi HP. Characteristics of thermally-enhanced bentonite grouts for geothermal heat exchanger in south Korea. Sci China Ser E Technol Sci. 2010;53(1):123–12. https://doi.org/10.1007/s11431-009-0413-9.
Lee C, Min S, Kang SH, Sohn B, Choi H. Comparison of effective thermal conductivity in closed-loop vertical ground heat exchangers. Appl Therm Eng. 2011;31:3669–367. https://doi.org/10.1016/j.applthermaleng.2011.01.016.
Li Z, Zhang K, Guo X, Liu J, Cheng X, Du J. Study of the failure mechanisms of a cement sheath based on an equivalent physical experiment. J Nat Gas Sci Eng. 2016;31:331–3. https://doi.org/10.1016/j.jngse.2016.03.037.

Liu ZR, Ye WM, Zhang Z, Wang Q, Chen YG, Cui YJ. Particle size ratio and distribution effects on packing behaviour of crushed gmz bentonite pellets. Powder Technol. 2019;351:92–101. https://doi.org/10.1016/j.powtec.2019.03.038.
Madsen FT, Müller-Vonmoos M. The swelling behaviour of clays. Appl Clay Sci. 1989;4(2):143–56.
Mahmoud M, Ramadan M, Pullen K, Abdelkareem MA, Wilberforce T, Olabi AG, et al. A review of grout materials in geothermal energy applications. Int J Thermofluids. 2021;10:100070. https://doi.org/10.1016/j.ijft.2021.100070.
Marshland A. Discussion, principles of measurement. Field Instrumentation in Geotechnical Engineering. 1973: pp 531–532.
Mikkelsen PE. Cement-bentonite grout backfill for borehole instruments. Geotech News. 2002;20(4):38–42.
Oesterholt F, Bloemendal M, van Bel N, van den Brand T. Milieuwinst en waterkwaliteitseffecten van thermische energie uit drinkwater. H2O: Tijdschrift voor Watervoorziening en Waterbeheer. 2018.
Ogden FL, Ruff JF. Setting time effects on bentonite water-well annulus seals. J Irrig Drain Eng. 1991;117(4):534–45.
Ogden FL, Ruff JF. Strength of bentonite water-well annulus seals in confined aquifers. J Irrig Drain Eng. 1993;119(2):242–50.
Pellegrini M, Bloemendal M, Hoekstra N, Spaak G, Gallego AA, Comins JR, et al. Low carbon heating and cooling by combining various technologies with aquifer thermal energy storage. Sci Total Environ. 2019;665:1–10. https://doi.org/10.1016/j.scitotenv.2019.01.135.
PUSH-IT. Piloting underground storage of heat. 2025. https://www.push-it-thermalstorage.eu. Accessed 16 Oct 2025.
Qin PJ, Fisonga M, Deng YF, Cui YJ, Ye WM. Mechanical properties of teguline clay pellet mixtures during continuous oedometric compression. Appl Clay Sci. 2024;260:107535. https://doi.org/10.1016/j.clay.2024.107535.
Roy P, Morris JP, Walsh SD, Iyer J, Carroll S. Effect of thermal stress on wellbore integrity during CO2 injection. Int J Greenhouse Gas Control. 2018;77:14–26. https://doi.org/10.1016/j.ijggc.2018.07.012.
van der Schans M. Reliable and affordable backfilling of boreholes in closed thermal energy systems. 2021. https://www.kwrwater.nl/en/projecten/betrouwbaar-en-betaalbaar-aanvullen-boorgaten-voor-gesloten-bodemenergiesystemen.
Shadravan A, Schubert J, Amani M, Teodoriu C. Using fatigue-failure envelope for cement-sheath-integrity evaluation. SPE Drill Completion. 2015;30(01):68–75.
SIKB. Protocol 2101: Mechanisch boren. 2021. https://www.sikb.nl/doc/BRL2100/Protocol_2101_v4_1_20211102.pdf. Accessed on 1 Jul 2025.
Teodoriu C, Falcone G. Comparing completion design in hydrocarbon and geothermal wells: the need to evaluate the integrity of casing connections subject to thermal stresses. Geothermics. 2009;38(2):238–46. https://doi.org/10.1016/j.geothermics.2008.11.006.
Thiercelin M, Dargaud B, Baret J, Rodriquez W. Cement design based on cement mechanical response. SPE Drill Completion. 1998;13(04):266–73. https://doi.org/10.2118/52890-PA.
Top Sector Energie. Encapsulation of bentonite pellets for controlled downhole placement and sealing. 2018. https://projecten.topsectorenergie.nl/projecten/encapsulation-of-bentonite-pellets-for-controlled-downhole-placement-and-sealing-34625. Accessed on 6 June 2024.
van Nimwegen D, van't Westende J, Omrani PS, Wasch L, Peters E. Feasibility study for combined geothermal-ates completions. 2022.
Wu Y, Patel H, Salehi S. Thermal considerations of cement integrity in geothermal wells. In: The 45th Workshop on Geothermal Reservoir Engineering. Stanford; 2020.
Xu H, Peng N, Ma T, Yang B. Investigation of thermal stress of cement sheath for geothermal wells during fracturing. Energies. 2018;11(10):2581. https://doi.org/10.3390/en11102581.
Zhang S, Qiao W, Li Y, Xi K, Chen P. Effect of additives on the rheological and mechanical properties of microfine-cement-based grout. Adv Mater Sci Eng. 2019;1:1931453.
Zwamborn M, Beernink S, Kleinlugtenbelt R, Oerlemans P, Pothof I, Star K, Dinkelman D, Bergen F, et al. Ht-ates systems in district heating networks, a Dutch benchmark study. 2022.

Publisher's Note